Visualizing Specific Cross-Protomer Interactions in the Homo-Oligomeric Membrane Protein Proteorhodopsin by Dynamic-Nuclear-Polarization-Enhanced Solid-State NMR

Jakob Maciejko,[†] Michaela Mehler,[†] Jagdeep Kaur,[†] Tobias Lieblein,[‡] Nina Morgner,[‡] Olivier Ouari,[§] Paul Tordo,[§] Johanna Becker-Baldus,[†] and Clemens Glaubitz*,[†]

[†]Institute for Biophysical Chemistry & Centre for Biomolecular Magnetic Resonance and [‡]Institute for Physical and Theoretical Chemistry, Goethe-University Frankfurt, 60438 Frankfurt am Main, Germany

[§]Aix-Marseille Université, CNRS, ICR, UMR 7273, 13013 Marseille, France

S Supporting Information

ABSTRACT: Membrane proteins often form oligomeric complexes within the lipid bilayer, but factors controlling their assembly are hard to predict and experimentally difficult to determine. An understanding of protein−protein interactions within the lipid bilayer is however required in order to elucidate the role of oligomerization for their functional mechanism and stabilization. Here, we demonstrate for the pentameric, heptahelical membrane protein green proteorhodopsin that solid-state NMR could identify specific interactions at the protomer interfaces, if the sensitivity is enhanced by dynamic nuclear polarization. For this purpose, differently labeled protomers have been assembled into the full pentamer complex embedded within the lipid bilayer. We show for this proof of concept that one specific salt bridge determines the formation of pentamers or hexamers. Data are supported by laser-induced liquid bead ion desorption mass spectrometry and by blue native polyacrylamide gel electrophoresis analysis. The presented approach is universally applicable and opens the door toward analyzing membrane protein interactions within homo-oligomers directly in the membrane.
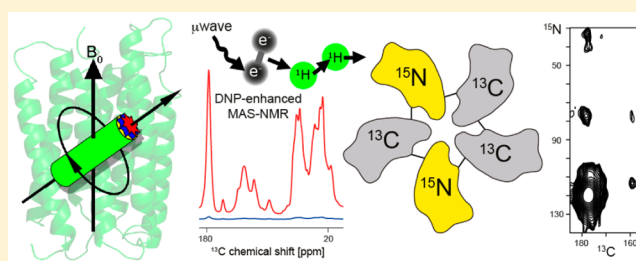
INTRODUCTION

Oligomerization through noncovalent interactions is a common structural characteristic of proteins. It is generally believed to be advantageous for structural stability of individual subunits as well as for regulation of functionality. Many proteins show cooperativity in substrate binding that can only be mediated by intersubunit cross-talk.[1] In the case of membrane proteins, (homo-)oligomerization is often observed and can be of direct functional importance,[2] but its role is disputed since complex-forming monomers are often functional as well. For example, self-association of G-protein-coupled receptors (GPCRs) is debated, as it probably depends on the type of receptor as well as on the stage of its life cycle.[3] Such "facultative" homo-oligomerization[4] is also observed for microbial rhodopsins.[5] Different oligomeric states have been reported, such as trimers for the archaeal bacteriorhodopsin (BR)[6] and for the bacterial *Gloeobacter* rhodopsin.[7] In contrast, channelrhodopsin-2 forms functionally important dimers,[8] and for green and blue proteorhodopsin (PR), pentamers and hexamers have been observed.[9,10]

Frequently used methods to assess the oligomeric state of self-association of membrane proteins include size exclusion chromatography (SEC), combined with multiangle light scattering (SEC−MALS), analytical ultracentrifugation, blue native−polyacrylamide gel electrophoresis (BN-PAGE), and,

most powerfully, mass spectrometric approaches, such as laser-induced liquid bead ion desorption (LILBID).[11,12] The arrangement of protomers with respect to each other can be derived, for example, from X-ray crystallography, cryo-EM, or pulsed EPR spectroscopy. However, understanding the oligomerization mechanism requires the identification of key interactions at the protomer interfaces. Most data available so far were derived from the increasing number of membrane protein crystal structures, which are sometimes difficult to interpret, as it is challenging to disentangle biologically relevant interactions from those induced by crystal contacts.[13,14] A further complication arises from the often observed limited protein integrity in detergent micelles.[15] Therefore, complementary spectroscopic data in the membrane environment are highly desirable. In principle, solid-state NMR, in particular based on magic angle sample spinning (MAS), could provide such interaction data, which is demonstrated here for the case of the green proteorhodopsin pentamer.

Solid-state NMR has been shown to offer a powerful approach for linking functional mechanisms with structure and dynamics of membrane proteins embedded within lipid bilayers,[16,17] which is best illustrated in the field of retinal proteins with applications stretching from the visualization of finest perturbation within the

retinal cofactor[18,19] via resonance assignments[20,21] to 3D structure determination.[22] Although direct protein interactions within membrane protein homodimers have not been studied, the possibility to probe protein–protein contacts by solid-state NMR has been shown in a few cases by directly observing interpeptide dipole couplings[23] or indirectly through paramagnetic relaxation enhancement.[24] In the case of amyloid fibrils, mixed-labeled samples were used to obtain interprotein distance constraints.[25,26] An improvement in sensitivity of MAS NMR by orders of magnitude has been achieved by dynamic nuclear polarization. The most used mechanism so far is based on the cross-effect through which a dipole-coupled electron pair creates a non-Boltzmann magnetization at nearby protons under microwave irradiation. This polarization is distributed throughout the sample via spin diffusion causing an almost homogeneous nuclear magnetization increase (for a recent review see, for example, ref 27). This approach has been shown to be most powerful for hypothesis-driven studies under cryogenic conditions, as demonstrated first for bacteriorhodopsin and later also for other membrane proteins.[28–30]

Green proteorhodopsin (*e*BAC31A08 variant) is a light-driven proton pump[31] and part of a large protein family, whose members were identified through metagenomic screens of microbial communities from sea surface ecosystems.[32] Their prevalent occurrence makes retinal-based phototrophy a very important bioenergetic factor.[33] Especially, the green-absorbing variant of PR has been extensively studied through advanced biophysical methods,[34] and solid-state NMR, in particular, has been applied to resolve secondary structure and dynamics within the lipid bilayer[35] and to elucidate important details of its functional mechanism and color tuning.[36–38] So far, no X-ray data but a low-resolution backbone structure based on solution-state NMR of the green PR monomer in detergent[39] has been reported. AFM studies have shown that green PR assembles into radial hexamers and pentamers in 2D crystalline samples[9] (Figure 1a). The latter was confirmed by LILBID-MS on green PR solubilized in dodecyl *β*-maltoside (DDM), where it forms predominantly pentamers.[40] Other studies have also confirmed its high oligomeric state and reported the relative protomer orientation within the complex based on EPR spectroscopy.[41,42] However, the interactions between the protomers are unknown for the reasons outlined above.

We have therefore taken this open question as a showcase to illustrate how such information could be obtained. The underlying experimental concept is illustrated in Figure 1a. By dis- and reassembling of homo-oligomeric green PR oligomers, mixed-labeled ^{13}C–^{15}N complexes can be created that show a unique isotope labeling pattern across their protomer interfaces. Using suitable solid-state NMR (ssNMR) methods such as ^{15}N–^{13}C TEDOR spectroscopy,[43,44] through-space dipole–dipole couplings indicative of specific cross-protomer contacts can be identified in this way. However, even a superficial consideration of such an approach will come to the conclusion that conventional ssNMR will be highly challenging, since oligomer mixing follows a statistical distribution, resulting in only a reduced number of mixed-labeled interfaces. Therefore, sensitivity enhancement based on dynamic nuclear polarization (DNP) using, for example, AMUPol as polarizing agent (Figure 1b)[45] is indispensable. The labeling scheme used here visualizes interprotomer salt bridges (Arg/Lys–Asp/Glu) as supposed from 3D crystal structures of blue PR.[10] Single-site mutations are introduced for assigning the observed contacts and to probe their role for complex formation by LILBID-MS[12] and BN-PAGE.[46]
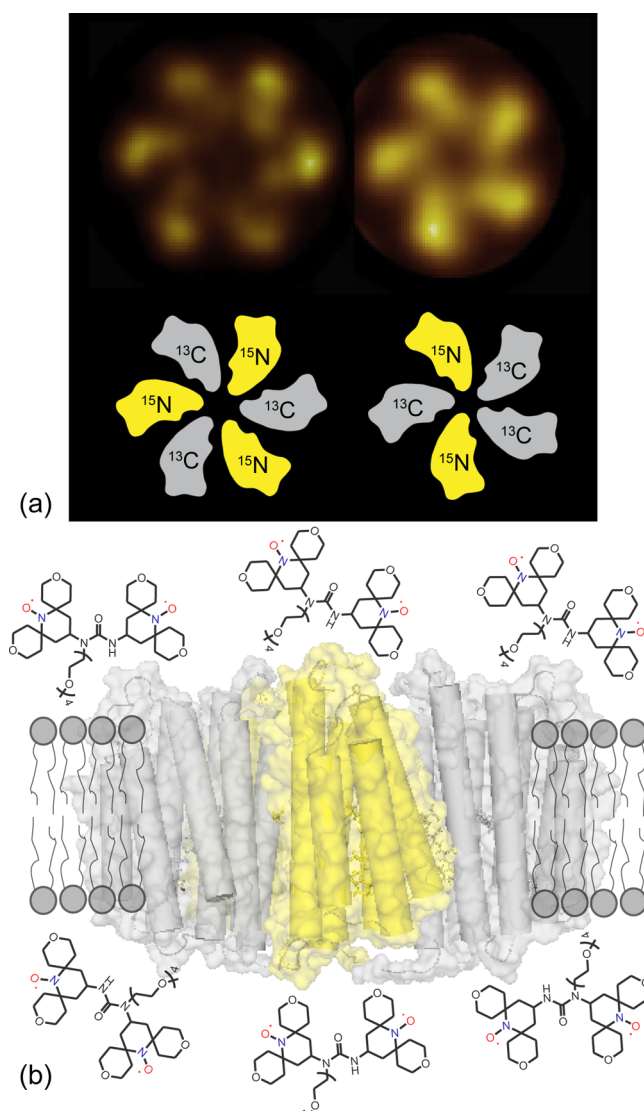

Figure 1. (a) AFM images of green PR oligomers.[9] Predominately hexamers are found in 2D crystals, while mainly pentamers occur in proteoliposomes and DDM micelles.[9,40] Cross-protomer interactions could be identified by ^{13}C–^{15}N through-space correlation spectroscopy on samples assembled from ^{13}C- and ^{15}N-labeled protomers. (b) The size of the complex within lipid bilayers (5 × 7 or 6 × 7 transmembrane helices) and the expected low number of interacting spin pairs make the use of dynamic nuclear polarization for signal enhancement indispensable, which requires sample doping with biradicals such as AMUPol.[45]

We found that one particular salt bridge plays a significant role for self-assembly and serves as an oligomerization switch between the native pentameric and the hexameric state of green PR. Our findings are discussed with respect to methodological aspects of DNP, in the context of known structures of proteorhodopsin complexes, with regard to factors controlling complex formation and finally with respect to the functional role of the oligomeric state of green PR.

■ RESULTS

Creating Mixed-Labeled Green PR Oligomers. In order to identify ^{13}C–^{15}N side chain contacts through DNP-enhanced TEDOR experiments, a procedure for assembling green PR oligomers consisting of neighboring ^{13}C and ^{15}N protomers had
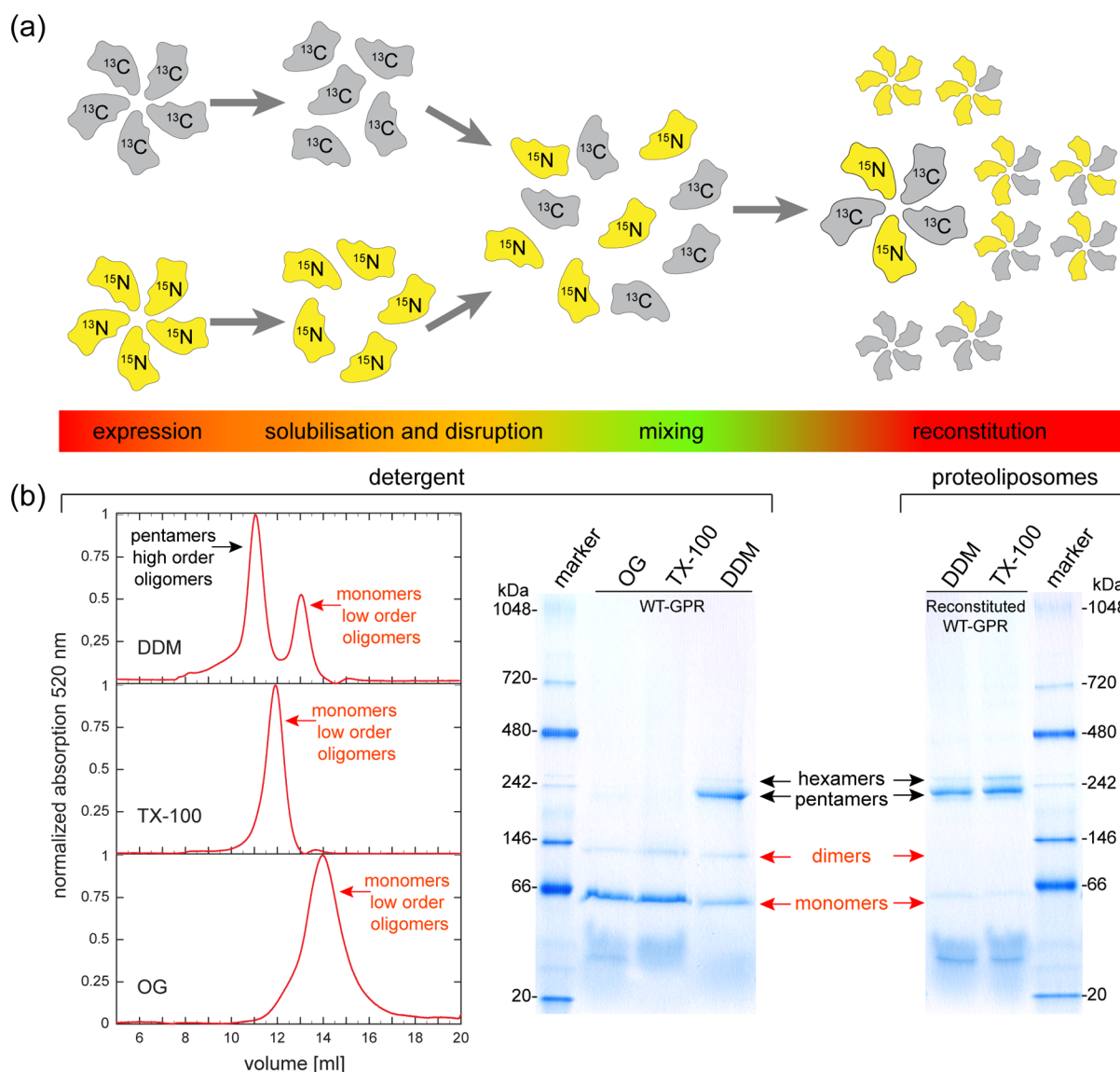
Figure 2. (a) Chart illustrating the general procedure for the production of mixed, high-order oligomers: Differently labeled proteins are separately expressed and disrupted by solubilization with a suitable detergent. These disrupted protomers are mixed in a 1:1 ratio and reconstituted into proteoliposomes, assembling into mixed-labeled pentamers [see Figure 3 and Table S1 (Supporting Information, SI) for mixing statistics]. (b) Size-exclusion chromatography and BN-PAGE analysis of green PR oligomers under different conditions: In BN-PAGE, pentamers appear as the most abundant high-order oligomeric state in DDM. This was additionally verified by LILBID-MS (Figure 5c). Solubilization with TX-100 or OG is sufficient to disrupt green PR into monomers. However, pH-titration experiments indicate that the treatment with TX-100 is preferable for the protein (Figure S1, SI). After reconstitution into proteoliposomes from TX-100 or DDM, green PR assembles back to mainly pentamers and a small fraction of hexamers.

to be established. The basic idea is illustrated in Figure 2a: Differently labeled green PR complexes are separated into monomers or low-order oligomers by suitably chosen detergents, mixed, and reconstituted into a lipid bilayer upon which mixed complexes are formed.

The largest number of interprotomer $^{13}C-^{15}N$ interfaces is obtained for complete disruption of the green PR oligomers into monomers. We have therefore solubilized and purified green PR in different detergents [DDM, TritonX-100 (TX-100), and octyl glycoside (OG)] and assessed its oligomeric state.

The size-exclusion chromatogram of green PR in DDM recorded at 520 nm reveals high- and low-order oligomers with a predominant peak eluting at ~11 mL and a smaller peak eluting at ~13 mL (Figure 2b). Since it is difficult to identify the size of membrane protein complexes within their detergent micelles by size exclusion chromatography,[47] we have also used BN-PAGE

and mass spectrometry. BN-PAGE (Figure 2b) shows one main pentamer population, which is confirmed by LILBID mass spectrometry (Figure 5c) in agreement with earlier studies.[40] This verification by LILBID, a well-tested and unambiguous method for determining the mass of macromolecular complexes, demonstrates that BN-PAGE analysis offers a reliable assessment of the oligomeric state of green PR. Other studies have interpreted the observed high-order oligomers as hexamers, but none of the methods used in these reports allows discriminating hexamers from pentamers.[41,42,48] In contrast to DDM, exclusively low-order oligomers are found in size-exclusion chromatograms with TX-100 and OG, which are identified as mainly monomers in BN-PAGE (Figure 2b). The different elution volumes of these monomers and low-order oligomers in DDM, TX-100, and OG are caused by their differing micelle dimensions.[49,50] These results suggest that TX-100 and

OG are able to disrupt green PR into low-order oligomers, which would allow sufficient mixing of differently labeled protomers.

To examine whether the disrupting detergents have further effects on green PR, pH titrations of the retinal absorption band were conducted in order to determine the pK_a of the primary proton acceptor Asp97 (Figure S1, SI). Protein samples either treated with DDM or TX-100 show similar pK_a values (6.9 and 6.8), which are comparable to previously reported results.[31,36,51] On the contrary, a shift to a much more basic pK_a can be observed (8.0) when green PR is solubilized in OG. This deviation suggests that OG has a significant conformational impact on the protein, affecting the interaction between the Schiff-base-linked retinal chromophore and the opsin binding pocket in some way. Therefore, to ensure milder conditions during sample preparation, TX-100 was favored for oligomer disruption, as it presumably keeps green PR in a conformation that correlates more with its native structure.

After solubilization with TX-100, differently labeled monomers were mixed in a 1:1 ratio followed by reconstitution into DMPC/DMPA (9:1) lipid bilayers. Independent of the use of DDM or TX-100, mainly pentamers, but no monomers, are found within the liposomes upon reconstitution, as observed by BN-PAGE (Figure 2b). It is important to note that the reconstituted membrane protein complex is not fully solubilized for BN-PAGE and a small amount of DDM is only used to assist substituting lipids by Coomassie BBG-250 as charge shift agents. The observed oligomeric state, therefore, indeed reflects the complex size within liposomes (see also Figure S6, SI). Using this approach, samples were prepared in which the pentamer consists of (i) [13]C- and ^{15}N-GPR protomers ([CN]-GPR), (ii) ^{13}C-GPR and ^{15}N-Arg-Lys-GPR protomers ([CN(Arg,Lys)]-GPR), (iii) ^{15}N-GPR ([NN]-GPR), and (iv) ^{13}C-GPR ([CC]-GPR). The latter two are control samples for analyzing [13]C–[15]N contacts arising from naturally occurring [13]C- or ^{15}N-isotopes. In order to reduce this contribution, all ^{15}N-labeled protomers were ^{13}C-depleted by using [[12]C$_6$]glucose (99.5%) as carbon source, resulting in 50% reduction of the ^{13}C background.
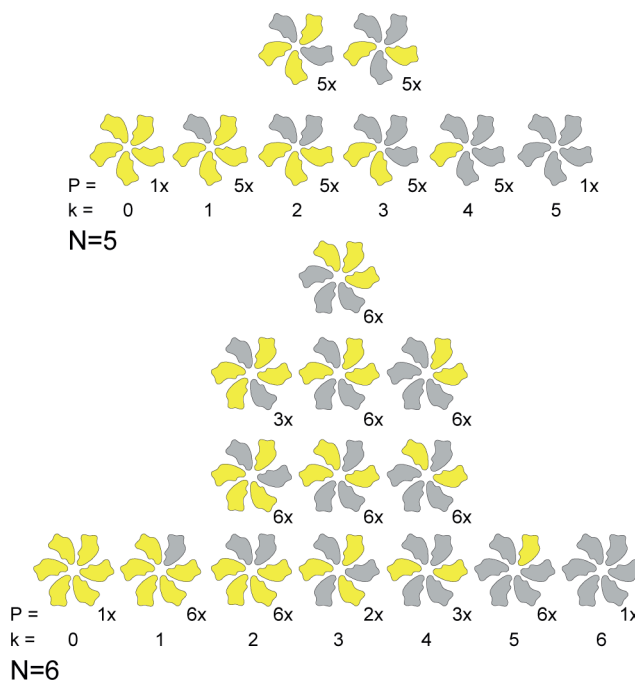
Statistical Analysis. Assembling [CN]-GPR from [13]C (gray) and [15]N (yellow) labeled monomers (Figure 2) results in a distinct number of configurations, which are differently populated. The population P for a particular configuration is given by

$$P(N,k) = \frac{N!}{k!(N-k)!} \tag{1}$$

where N is the number of green PRs in the complex (5 or 6) and k is the number of ^{13}C-labeled protomers within the ^{15}N-labeled complex. The different configurations are illustrated in Figure 3. Each configuration results in a particular number of [13]C–[15]N interfaces, $I(N,k)$. The average number of interfaces per complex is obtained by

$$I^{Avg} = \frac{\sum_{k=1}^{N} P(N,k)\, I(N,k)}{\sum_{k=1}^{N} P(N,k)} \tag{2}$$

but only half of them are unique interfaces (N → C vs C → N). A statistical analysis of the pentamer and the hexamer is explicitly given in Table S1 (SI). For a pentamer, eight different configurations are possible, resulting in an average number of 2.5 N–C interfaces per complex, of which 1.25 contribute to the [15]N–[13]C TEDOR spectra. Similarly, the average is 3.0 interfaces for the hexamer, of which 1.5 are TEDOR active.

Figure 3. Assembling [CN]-GPR from [13]C (gray) and [15]N (yellow) labeled monomers (see Figure 2) results in 8 different pentamer and 14 hexamer configurations, which are differently populated. The average number of NC interfaces per pentamer and hexamer is 2.5 and 3.0, respectively, but only half of them are unique (N → C vs C → N) (see Table S1, SI). This means that even for large amounts of available protein, the number of potential cross-protomer interactions involving residues with ^{13}C-labeled side chains on the one side and ^{15}N-labeled side chains on the other is small, making the use of DNP indispensable.

DNP-Enhanced [15]N–[13]C TEDOR Through-Space Correlation Spectroscopy. DNP-enhancement was achieved by doping the sample with the biradical polarizing agent AMUPol.[45] A 60-fold signal increase was observed for green PR when comparing [13]C−CP spectra obtained with and without microwave irradiation (Figure 4a). This makes AMUPol currently the best compound for DNP-enhanced ssNMR on membrane proteins. Such a sensitivity enhancement enabled us to perform [15]N−[13]C TEDOR experiments on the mixed oligomers [CN]-GPR and [CN(Arg, Lys)]-GPR as well as on the controls [CC]-GPR and [NN]-GPR (Figure 4b). TEDOR spectra visualize through-space dipole−dipole contacts between ^{13}C and ^{15}N spins. The mixing time (6.25 ms) was adjusted to maximize the signals of expected long-range cross-protomer couplings. All four spectra show distinct natural abundance cross-peaks arising from N−CO and N−CA single bond contacts but also from long-range N−CX couplings. Arginine intraresidue [13]C−[15]N contacts between Arg-Nη,ε and Arg-Cζ are also detected for samples containing ^{13}C-labeled protomers. These cross-peaks occur because ^{15}N-labeled protomers still contain ~0.5% [13]C natural abundance despite depletion with ^{12}C, while the ^{15}N natural abundance in ^{13}C-labeled protomers accounts for ~0.4%. Therefore, the pentamers in the [CN]-GPR sample contain on average six N−CA and six N−CO spin pairs (Table S2, SI). The resulting cross-peak pattern is a superposition of the spectra from [CC]- and [NN]-GPR. Further details are provided together with the full spectra in Figure S2 (SI).

Comparing the [CN]-GPR spectrum with both control spectra reveals five additional cross-peaks (i−v), which consequently must come from cross-protomer [13]C−[15]N
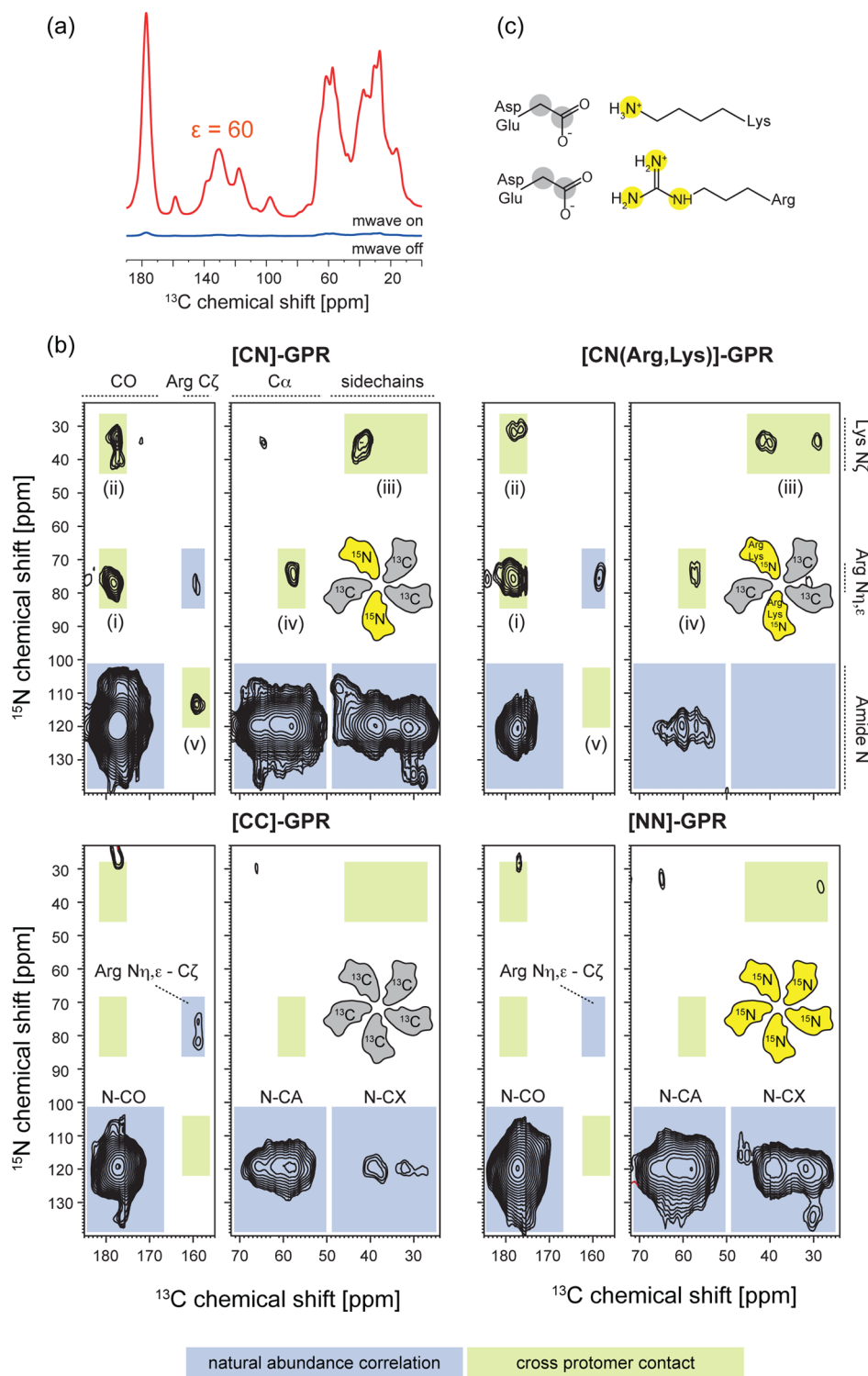
Figure 4. (a) DNP enhancement shown for a ^{13}C−CP spectrum of green PR incubated with 20 mM AMUPol. Upon microwave irradiation, a 60-fold sensitivity enhancement is obtained. (b) DNP-enhanced ^{15}N−^{13}C-TEDOR spectra (t_{mix} = 6.25 ms) of [CN]-GPR and [CN(Arg,Lys)]-GPR and control samples [CC]-GPR and [NN]-GPR. All spectra show cross-peaks arising from natural abundance intramolecular backbone ^{13}C−^{15}N-contacts. Additional cross-peaks labeled i−v are observed in [CN]-GPR and [CN(Arg,Lys)]-GPR. They can be assigned to cross-protomer contacts: peak i represents a through-space correlation between Arg and Asp/Glu, while peak ii arises from Lys-Asp/Glu contacts (see the text and Figure S2, SI). (c) These cross-protomer cross-peaks show that salt bridges between Asp/Glu and Arg/Lys must exist at the oligomerization interfaces.

contacts. The signals are found in the ^{15}N chemical shift range of arginine and lysine, indicating that these residues play a distinct role for cross-protomer interactions. This is confirmed by the selectively labeled [CN(Arg,Lys)]-GPR sample, which displays the same cross-protomer correlation pattern as [CN]-GPR.

Cross-peaks i and ii reveal that the ^{15}N resonance of Arg-Nη,ε and Lys-Nζ correlates with ^{13}C resonances of carboxyl groups from Asp-Cγ and/or Glu-Cδ, indicating possible cross-protomer salt bridge contacts between these residues (Figure 4c). Besides these potential salt bridge contacts, further cross-peaks are visible
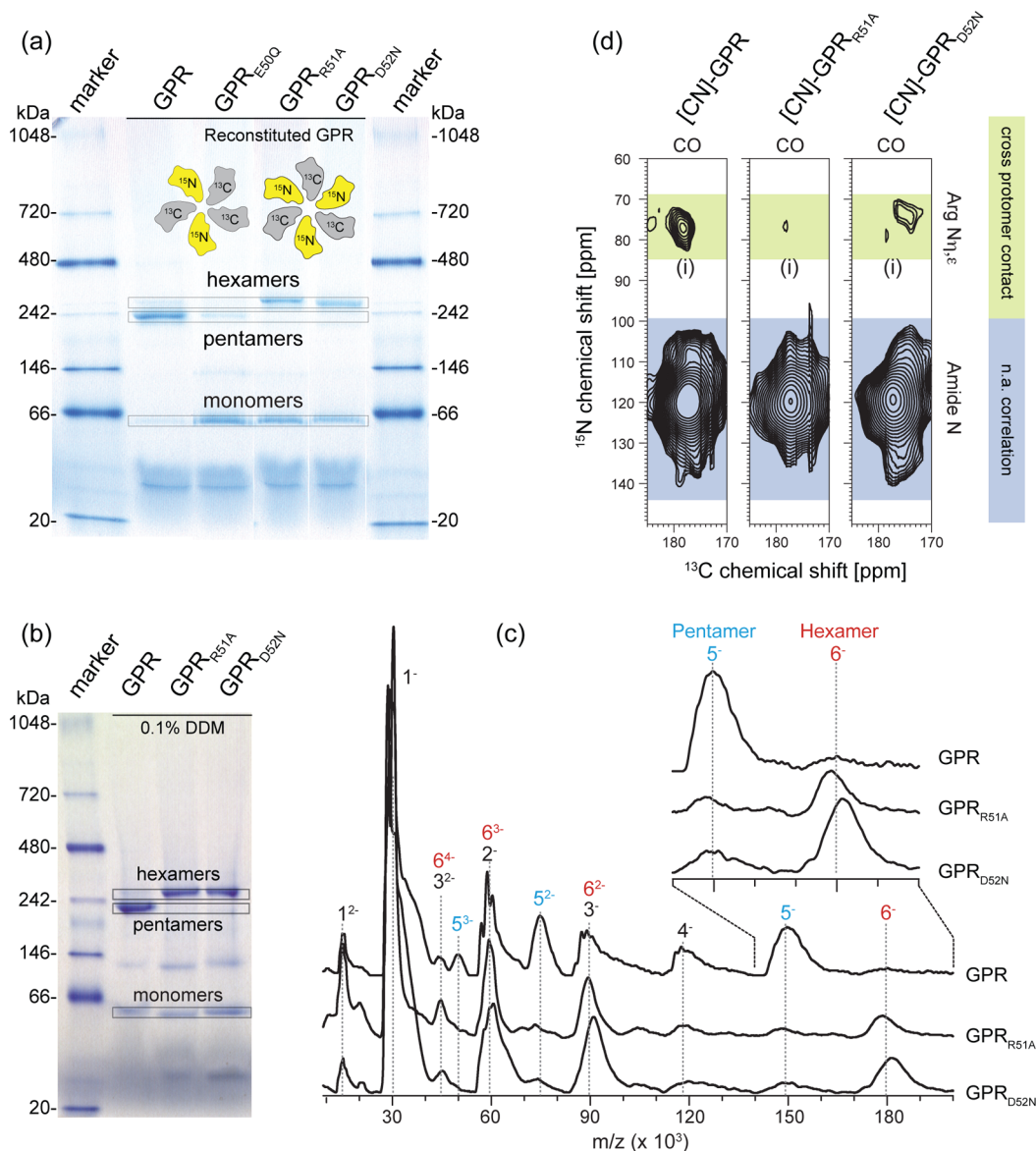
Figure 5. (a) Effect of mutations E50Q, R51A, and D52N on the oligomerization of green PR within lipid bilayers, as seen by BN-PAGE analysis. In contrast to pentameric green PR, mainly monomers (GPR_{E50Q}) and hexamers (GPR_{R51A}, GPR_{D52N}) form upon mutation. (b) The same behavior is observed for GPR_{R51A} and GPR_{D52N} by BN-PAGE in DDM (Figure S4a, SI) and (c) by LILBID-MS (GPR occurs at charge states −1 to −4, indicated in blue for the pentamer and red for the hexamer). The BN-PAGE results agree with size exclusion chromatography (Figure S4b, SI). All mutants displayed similar pK_a values of the primary proton acceptor of approximately 7 (Figure S4c, SI). (d) DNP-enhanced 2D-TEDOR spectra ($t_{mix} = 6.25$ ms) of [CN]-GPR_{R51A} and [CN]-GPR_{D52N} compared to [CN]-GPR. For [CN]-GPR_{R51A} cross-peak i almost disappears, showing that this correlation arises from a coupling between R51 and E50 or D52. In the case of [CN]-GPR_{D52N}, peak i is significantly shifted. Full spectra are shown in Figure S3 (SI).

for [CN]-GPR. Contact iii could be attributed to Lys-Nζ being in close proximity to aliphatic side chain carbons of the neighboring protomer, but it also could have contributions from natural abundance intraresidue contacts between Lys-Nζ and Lys-Cε. Contact iv could be caused by correlations between Arg-Nη,ε and carbons of other interface residues, such as serine or threonine, and contact v could arise from Arg-Cζ−backbone correlations.

These data show that DNP-enhanced TEDOR spectra allow detecting $^{13}C-^{15}N$ contacts, such as those arising from salt bridges across the protomer interface of oligomeric membrane proteins. However, additional data are needed to assign these cross-peaks to specific residues and to elucidate their importance for oligomerization. While the first problem could in principle be solved by more complex labeling schemes, the second would require suitably chosen single-site mutations, which also allow cross-peak identification. We have therefore decided to use the mutation approach and focus here for this proof of concept study on salt bridges formed between Arg and Asp and/or Glu. Potential candidates could be identified by rationalizing the location and orientation of Arg and Asp/Glu on the green PR surface, as predicted by structural models, and by assuming different protomer arrangements within the oligomer. The number of potential contacts is further reduced by taking into account that green PR assembles into radial pentamers in which helices A and B point inside and form contact interfaces with neighboring helices A′ and B′.[42] The most promising candidates to form cross-protomer pairs are therefore R51 and E50/D52 (Figure 7a). In order to verify this assumption, we have therefore

introduced the mutations R51A, E50Q, and D52N into green PR.

Importance of Cross-Protomer Contacts for Oligomerization. The single mutants GPR$_{E50Q}$, GPR$_{R51A}$, and GPR$_{D52N}$ were reconstituted into liposomes and subjected to BN-PAGE analysis, which reveals a strongly altered oligomerization behavior (Figure 5a). Upon introducing E50Q, only monomers can be detected. Therefore, E50 must play an important role in the formation of high-order oligomers. In the cases of R51A and D52N, hexamers instead of pentamers are observed, along with a monomer subpopulation. This shift toward hexamers is confirmed by BN-PAGE and especially LILBID-MS analysis of both mutants solubilized in DDM (Figures 5b,c). Both residues are therefore involved in an "oligomerization switch" controlling pentamer or hexamer formation. A comparison of BN-PAGE and SEC data of all mutants solubilized in DDM is provided in Figure S4a,b (SI). All mutants display a similar pH-titration behavior of their optical absorption spectra, which shows that the pK_a of the primary proton acceptor is not affected (Figure S4c, SI). This demonstrates that these mutations do not have any significant conformational impact on the protein.

Mixed complexes [CN]-GPR$_{R51A}$ and [CN]-GPR$_{D52N}$ were prepared in order to analyze these hexameric mutants by TEDOR experiments (Figure 5d). For [CN]-GPR$_{R51A}$, an almost complete loss of cross-peak i (Arg-Asp/Glu) is observed, compared to [CN]-GPR, confirming that R51 is indeed taking part in this cross-protomer network. In the case of [CN]-GPR$_{D52N}$, cross-peak i disappears and a new resonance with reduced intensity and a ^{13}C chemical shift reduced by 4 ppm is detected. This observation confirms the involvement of D52 and the formation of a cross-protomer salt bridge R51−D52′. The new peak can be explained by the different ^{13}C chemical shift of N52−Cγ in the mutant, which is close in space to R51. In the case of GPR$_{E50Q}$ mixed-labeled complexes for a NMR analysis could not be prepared, since it decays into monomers. However, considering that E50 and D52 are located opposite to R51 in the pentamer, an additional electrostatic cross-protomer coupling between E50 and R51 can be postulated. On the other hand, R51 is not likely the primary coupling partner of E50, as the corresponding mutation R51A leads to hexamers but not exclusively to monomers.

Estimating the Distance between R51 and D52′. The distance between R51 and D52′ has been estimated from a ^{15}N-detected TEDOR buildup curve. All three nitrogens of the R51 guanidinium group contribute to the integral intensity observed in the ^{15}N-detected TEDOR spectra (Figure 6a), which could not be deconvoluted under our experimental conditions. Therefore, the observed TEDOR signal will depend on the dipole couplings between R51-Nε, -Nη1, -Nη2 and D52′-Cγ, resulting in an effective dipole coupling:[52,53]

$$D_{eff} = \sqrt{D_{C\gamma-N\eta1}{}^2 + D_{C\gamma-N\eta2}{}^2 + D_{C\gamma-N\varepsilon}{}^2} \qquad (3)$$

Dipole couplings involving D52′-Cβ can be neglected, as no such correlation has been detected in the 2D TEDOR spectra. The normalized buildup is shown in Figure 6b. The best fit is obtained for D_{eff} = 123 Hz (115−133 Hz in the 95% confidence interval). Interpreting D_{eff} in terms of distances would require prior knowledge about the orientation of both side chains with respect to each other. In the case of a linear arrangement, the observed D_{eff} would correspond to a distance of 3.68 Å between R51-Cζ and D52′-Cγ (see Figure S5b, SI). The observed TEDOR buildup also contains small contributions from
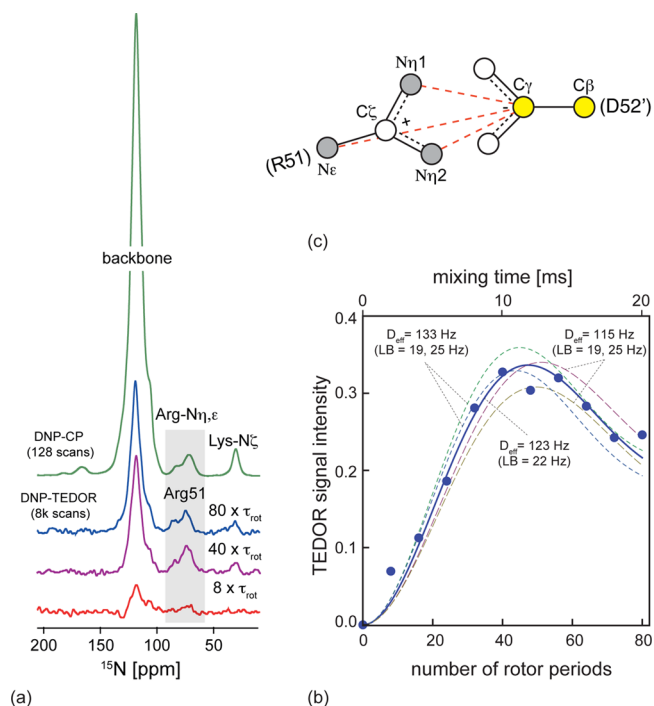

Figure 6. Estimation of the effective dipole coupling between R51 and D52 in [CN]-GPR. (a) A ^{13}C−^{15}N TEDOR buildup curve was measured by recording ^{15}N-detected TEDOR spectra with mixing times between 0 and 20 ms. (b) The buildup curve was normalized with respect to the cross-polarization intensity and fitted using a single effective NC dipole coupling constant, D_{eff}. The best fit is obtained for D_{eff} = 123 Hz [LB (a single-exponential relaxation damping parameter) = 22 Hz]. The 95% confidence intervals are 115−133 and 19−25 Hz for D_{eff} and LB, respectively. A RMSD contour plot and ^{15}N-T2′ data are shown in Figure S5 (SI). (c) The dipole−dipole couplings between D52-Cγ and R51-Nε, -Nη1, -Nη2 contribute to the effective coupling. See the text for further details.

intraresidue single-bond dipole couplings between R51-Cζ and Nε, Nη1, Nη2 due to residual ^{13}C and ^{15}N isotopes in ^{15}N- and ^{13}C-labeled protomers. Its contribution is estimated to be about 15% (Table S2, SI). The observed D_{eff} will therefore slightly underestimate the actual distances or rather overestimate the dipole couplings D_{eff} between R51 and D52′.

■ DISCUSSION

DNP-Enhanced MAS NMR Resolves Cross-Protomer Interaction within the Lipid Bilayer. The approach presented here is conceptually straightforward but technically challenging, which explains why such studies have not been carried out before. The first hurdle to overcome is to find a way to reassemble the oligomers from differently labeled protomers, but developing such protocols seems feasible in many cases. In addition to the work on microbial or archaeal rhodopsins, it has been shown for a number of other membrane proteins that well-chosen detergents can modulate their oligomeric state, which offers the opportunity to reassemble the full oligomer upon reconstitution into lipid bilayers. For example, GPCRs like rhodopsin or the β2-adrenoreceptor can be solubilized in monomeric form and dimerize within the membrane,[54−56] or the lipid regulator diacylglycerol kinase from *Escherichia coli* can be disrupted into monomers, but it reassembles into its active trimeric state.[57]

Although solid-state NMR is better suited than any other spectroscopic method to detect short-range through-space
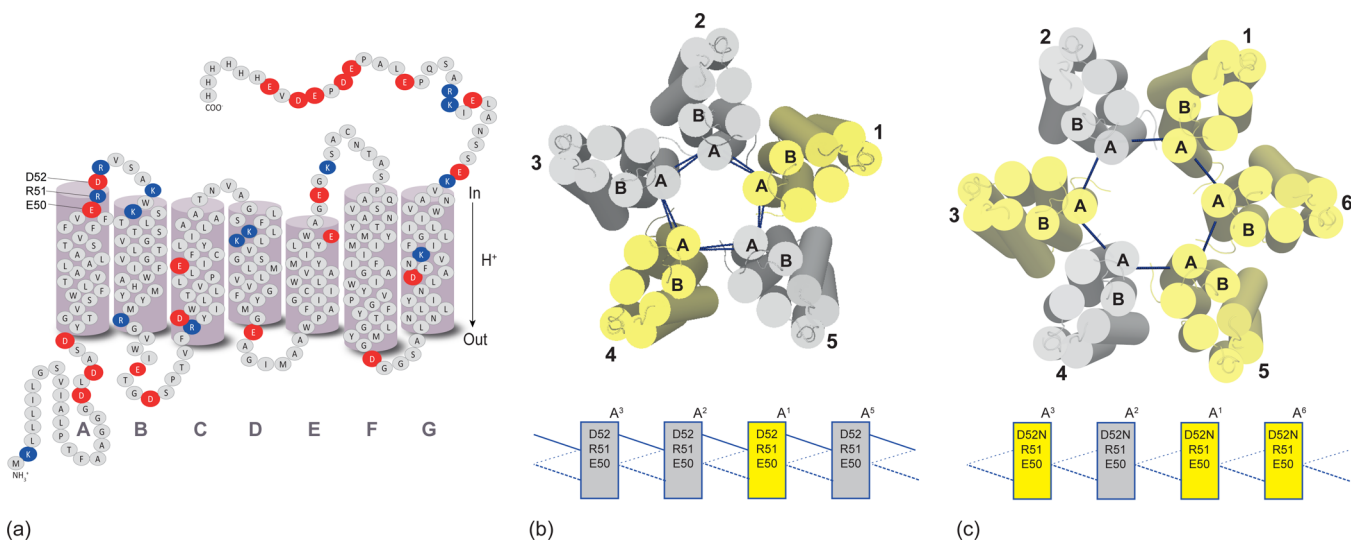
Figure 7. (a) Topology plot of green PR with Asp/Glu and Arg/Lys highlighted in red and blue, respectively. Residues E50, R51, and D52 in helix A control the oligomerization behavior. (b) The salt bridge R51−D52′ stabilizes the pentamer and acts as a "oligomerization switch" between pentamer and hexamer formation. E50 is essential for oligomerization and is postulated to be involved in electrostatic interactions with R51 and most likely via H-bonds with additional partners in the opposite helix A. (c) Introducing D52N (or R51A) destroys the pentamers and leads to hexamer formation. Pentamer and hexamer cartoons were created on the basis of the X-ray structures of two blue proteorhodopsin variants, which crystallized in both forms.[10]

contacts, such as salt bridges or H-bonds across protomer interfaces, the second hurdle arises from its intrinsically low sensitivity: Even if large amounts of membrane protein were available, the small number of cross-protomer spin pairs would be below the detection limit for conventional ssNMR. Here, only 1.25 uniquely labeled interfaces are found per pentamer, which results, foe example, in just 1.25 TEDOR-active R51−D52′ salt bridges (see Figure 3).

Fortunately, a solution is offered by using dynamic nuclear polarization, which provides in our case a 60-fold signal enhancement. Although current DNP-MAS NMR methods work better at lower than at higher fields and at low temperatures, which compromises somehow spectral resolution, the current study would simply be impossible based on conventional NMR: Performing the same 2D-TEDOR experiments without DNP would require 30 years instead of 3 days of NMR time. One side effect of DNP, which can be usually neglected in conventional NMR, is that also natural abundance cross-peaks contribute to the spectra pattern, as each [CN]-pentamer contains approximately six N−CA and six N−CO spin pairs (see Table S2, SI). Therefore, control experiments as carried out here are essential for such studies in order to differentiate cross-protomer correlations from natural abundance ones.

One Specific Cross-Protomer Salt Bridge Acts as an "Oligomerization Switch". Using these possibilities, we have identified one cross-protomer salt bridge in green PR as a proof of concept. The oligomer size in DDM as well as in proteoliposomes was identified as pentamer on the basis of LILBID-MS and BN-PAGE analysis. DNP-enhanced TEDOR and mutation data show the formation of a contact between R51 and D52′ (Figure 5). Both residues form a salt bridge, as the effective dipole coupling between both side chains indicates close spatial proximity (Figure 6). They are located at the cytoplasmatic side of helices A and A′ (Figure 7a). The cartoon in Figure 7b illustrates how these cross-protomer contacts form a beltlike interaction pattern, stabilizing the pentamer. Surprisingly, introducing the R51A and the D52N mutations leads to the

formation of hexamers (Figure 7c). The R51−D52′ salt bridge is therefore a key element for oligomer stabilization and acts as a "switch" between pentamer and hexamer formation.

One possible explanation is that the destabilization of the complex by destroying R51−D52′ is compensated by including a sixth protomer through which additional interactions are provided. These could be, for example, interactions involving interfacial Lys residues (as observed in Figure 4a) and/or residue E50. The latter must be involved in strong interactions, as the E50Q mutation leads to an almost pure monomer formation. For blue PR, a H-bonding network between E50 in A and opposite residues such as T60/63 in A′ have been suggested.[10] These interactions could provide a large enthalpy contribution, making the hexamer more stable than the pentamer if the R51−D52′ coupling is prevented.

Green PR has been reported to form predominantly hexamers under 2D crystallization conditions in DOPC,[9] but pentamers are dominating in DMPC/DMPA proteoliposomes. Additional control experiments show that reconstituting green PR into DOPC and DMPC/DMPA at different lipid-to-protein ratios and using different reconstitution methods mainly lead to pentamers except for conditions that are close to 2D crystallization (Figure S6, SI). Possible explanations could be that hexamer formation is geometrically favored in 2D crystals and that additional protein−protein contacts influence the oligomeric state. Indeed, it was shown by CD spectroscopy that green PR in 2D crystals shows signals that indicate additional (aromatic) protein−protein contacts, resulting also in higher thermal stability.[58]

3D crystal structures of two blue absorbing PRs have been reported.[10] The Med12BPR variant (57% identity to the green PR, PDB ID: 4JQ6) has been crystallized as the hexamer while two mutants of HOT75BPR variant (78% identity, PDB ID: 4KNF, 4JQ6) formed pentamers. In both structures, cross-protomer contacts like those reported here have been identified. The oligomer interface formed by helices A and B is predominantly conserved, but the interaction motif ERD at

position 50−52 is replaced by ERSD 50−53 (33−35) in MED12BPR. The essential salt bridge R51−D52′ would be therefore less favorable, since the additional Ser changes the relative side chain orientations of Arg51(33) and Asp52(35), which however could be compensated by including a sixth protomer in the ring-shaped complex. Furthermore, HOT75BPR has been crystallized from DDM at pH 6.5,[10] while 3D crystals of MED12BPR were obtained using the bicelle method at pH 4.5.[59] One cannot exclude that these different conditions shift the oligomeric state toward pentamers or hexamers. For a qualitative comparison with our NMR data, we have calculated the expected effective dipole couplings D_{eff} for the cross-protomer Arg−Asp salt bridges from these structures (Table S3, SI). For the two pentamers, average values of D_{eff} of 95.8 Hz (4KLY) and 108.0 Hz (4KNF) were obtained, while the hexamer shows a weaker coupling with D_{eff} = 75.8 Hz (4JQ6). The first two values agree relatively well with our experimentally determined coupling (Figure 6), especially if one considers that the proteins are not identical, that mutations were introduced (D97N and D97N/L105Q), and that a 3D crystal lattice is compared with a proteoliposome sample. The weaker coupling in the hexamer is also in line with our data, which shows that this unique salt bridge is especially needed to stabilized the pentameric but not the hexameric form.

Oligomeric State of Green PR Affects Its Photo-dynamics. Whether the oligomeric state of a particular membrane protein is functionally relevant or not is in many cases difficult to discern. It is especially difficult to disentangle detergent effects from the functional consequences of an altered oligomeric state in cases in which the complex size is controlled by the choice of certain detergents that are used at the same time as a membrane-mimicking environment for functional studies. For example, green PR was shown to be monomeric in DPC, in which its primary proton acceptor displays a different pK_a value compared to the pentamer formed in DDM. This observation has been attributed to its oligomeric state.[48] However, our own data illustrate that there are already large differences between monomeric green PR in Triton-X100 and in OG, which demonstrates that detergent effects alone can significantly modulate the properties of membrane proteins (Figure S1, SI).

It is therefore necessary to compare different oligomeric states in identical membrane environments. Our observation that the E50Q mutation, which does not have a direct effect on the optical properties of green PR (Figure S4, SI), disrupts complex formation altogether offers now the possibility to functionally compare monomeric with pentameric green PR directly within the lipid bilayer. However, an extensive study would be needed to ensure that this mutation itself does not directly influence the activity of green PR.

Alternatively, the photophysical properties of pentameric green PR in liposomes could be compared with those of smaller green PR (monomer−trimer) complexes formed in nanodisks that are assembled from the same lipids.[60,61] In both cases, a full photocycle with all characteristic intermediates has been observed.[60] However, the kinetics is strongly modulated, with the photocycle in nanodisks being twice as long as that of liposomes. The M-state in liposomes builds up much more slowly and has a shorter lifetime compared to that of nanodisks. This results in well-populated later N/O states in liposomes but less-populated N/O states in nanodisks. Of course, despite identical lipid compositions, nanodisks are not identical to liposomes, and an altered lateral pressure in the membrane might also affect the photocycle dynamics. However, these data represent currently the best possible analysis of the role of the oligomer in the functional properties of green PR while detergent effects or mutations are avoided and clearly demonstrate that pentameric green PR undergoes a faster photocycle, which would be of advantage for maintaining a stable proton motive force.

■ CONCLUSIONS

This study demonstrates for the first time that DNP-enhanced solid-state NMR can identify cross-protomer interactions within a homo-oligomeric membrane protein embedded within lipid bilayers. Our approach represents an essential extension of the so far limited portfolio of methods available to investigate interactions that govern membrane protein oligomerization and cross-protomer cross-talk. The labeling schemes can be easily tailored toward H-bond interaction pattern or less-specific hydrophobic contacts, so many applications can be envisaged.

■ MATERIALS AND METHODS

Sample Preparation. Samples were essentially prepared as described previously,[38] except for the oligomer mixing step.

Green PR Construct and Single Mutants. Green PR (*e*BAC31A08) was cloned into a pET27b(+) (Novagen) plasmid vector containing an additional C-terminal HSV sequence and hexahistidine-tag for purification. All single mutations were introduced to the wild-type green PR template vector by PCR amplification with overlapping mutagenic primers. Vectors were transformed into *E. coli* competent C43 (DE3) cells using the heat shock procedure and were subsequently plated on kanamycin-containing LB agar plates. Colonies were picked and grown in LB medium, and the plasmid DNA was isolated via an extraction kit. Sequences of green PR and all single-mutant constructs were verified at Eurofins MWG Operon.

Preparation of Mixed Samples. Expression of uniformly labeled green PR took place in *E. coli* C43 (DE3) cells using M9 minimal medium with [U-^{13}C]glucose or [^{15}N]ammonium chloride. Uniformly labeled ^{13}C and ^{15}N samples were expressed separately to create mixed samples that only exhibit interprotomer ^{13}C−^{15}N contacts and no intraprotomer ^{13}C−^{15}N contacts. Hence, ^{12}C-enriched glucose (99.5%) was used in uniformly ^{15}N-labeled samples instead of normal glucose to suppress ^{13}C natural abundance within a protomer. The selectively labeled sample was expressed in defined medium containing ^{15}N-labeled arginine and lysine as well as all remaining unlabeled amino acids and nucleotides. *E. coli* cells were grown until an OD600 of 0.6−0.8 was reached, whereupon protein expression was induced by the addition of IPTG and retinal. Cell disruption and Ni-NTA matrix purification was performed as previously described, except that green PR membranes were solubilized in 1.5% TX-100 for oligomer disruption and the protein was eluted in 0.1% TX-100. Subsequently, ^{13}C- and ^{15}N-labeled protomers were mixed in a 1:1 ratio and rotated overnight at 4 °C. After the mixing procedure, the protein was reconstituted into DMPC/DMPA (9:1) liposomes in a protein/lipid ratio of 2:1 (w/w). Using this approach, samples were prepared in which the green PR complex or its mutants consists of (i) ^{13}C- and ^{15}N-GPR protomers ([CN]-GPR), (ii) ^{13}C-GPR and ^{15}N-Arg-Lys-GPR protomers ([CN(Arg,Lys)]-GPR), (iii) ^{15}N-GPR ([NN]-GPR), and (iv) ^{13}C-GPR ([CC]-GPR). The latter two are control samples for analyzing ^{13}C−^{15}N contacts arising from naturally occurring ^{13}C- or ^{15}N-isotopes.

Analysis of Green PR. *BN-PAGE, SEC, and pH titrations.* Oligomeric states of green PR were analyzed via BN-PAGE and SEC. Preparation and electrophoresis of BN-PAGE gels (NativePAGE Novex Bis-Tris Gel 4−10%, 10 wells) were performed according to manufacturer's instructions (Life Technologies, NativePAGE Novex Bis-Tris). Samples were prepared with 3−4 μg of protein, 5 μL of 4× sample buffer [200 mM BisTris, 64 mM HCl, 200 mM NaCl, 40% (w/v) glycerol, 0.004% (w/v) Ponceau S, pH 7.2], 1 μL of 5% Coomassie Brilliant Blue G250 solution, and H$_2$O adjusted to a total volume of 20 μL. Additionally, 0.35% DDM was added to TX-100- or OG-solubilized samples as well as to DMPC/DMPA reconstituted samples.

Size-exclusion chromatography was executed on a Superdex 200 10/300 GL column (GE Healthcare) equilibrated in SEC buffer (150 mM NaCl, 50 mM MES, pH 7, 0.05% DDM/0.1% TX-100/0.8% OG). Prior to loading, green PR was transferred into SEC buffer, concentrated to ~50 μM, and filtered in order to remove aggregates. Protein elution from the column was monitored via absorption at 280 and 520 nm.

pH titrations on green PR were performed as previously described.[38] The protein was transferred into titration buffer (50 mM sodium citrate, 50 mM Na$_3$PO$_4$, 50 mM Tris, 50 mM boric acid, 100 mM NaCl, pH 7, 0.05% DDM/0.1% TX-100/0.8% OG). Starting at pH 7, titrations for a sample were carried out in both directions simultaneously by addition of 4 M NaOH or 4 M HCl and pH-dependent UV–vis spectra were recorded. The absorption maxima of the Schiff-base-linked retinal absorption were plotted against the respective pH values and fitted with a Boltzmann function.

LILBID Mass Spectrometry. For the LILBID-MS experiments, the protein was transferred into a salt-free buffer containing 50 mM ammonium acetate and 0.3% DDM. The green PR was concentrated to ~80 μM, using a 50 kDa cutoff filter (Amicon by EMD Millipore, Darmstadt, Germany). For each of the measurements, 3 μL of this solution was used.

The LILBID-MS measurements were carried out using previously published standard settings.[62] Briefly, a piezo-driven droplet generator (MD-K-130 by Microdrop Technologies GmbH, Norderstedt, Germany) produces droplets of 50 μm diameter at a repetition rate of 10 Hz. Those droplets contain the analyte of interest in the buffer–detergent solution described above. They are transferred to a two-stage differential vacuum chamber, where the droplets are irradiated by an IR laser pulse tuned to the absorption wavelength of water at 2.94 μm. This leads to an explosive expansion of the droplets and thus release of the analyte ion into the gas phase. The ions are accelerated by a pulsed electric field and mass-analyzed by a reflectron time-of-flight (TOF) mass spectrometer. LILBID has proven to be a soft method that can be employed to detect noncovalently bound complexes such as proteorhodopsin.[62,40]

The MS signal is recorded using the home-written program labview. For the spectra shown in this publication, the signals of 1000 droplets were averaged to improve the signal–noise ratio (SNR). Data processing was performed using the software *Mass*ign, allowing for signal calibration (using bovine serum albumin as standard and performing a two-point calibration), smoothing (using the method of moving average), and background subtracting.[63]

DNP-Enhanced ssNMR. *Sample Preparation.* Reconstituted protein samples were doped with a polarizing agent in order to achieve DNP signal enhancement. The proteoliposome pellet was covered with ~100 μL of a 20 mM AMUPol[45] solution (60% D$_2$O, 30% glycerol-d_8, 10% H$_2$O) and incubated overnight at 4 °C. The solution was completely removed before the sample was packed into a 3.2 mm ZrO$_2$ rotor.

DNP-Enhanced TEDOR Spectroscopy. DNP-enhanced MAS NMR spectra were recorded on a Bruker 400 DNP system consisting of a 400 MHz WB Avance II NMR spectrometer, a 263 GHz Gyrotron as microwave source, and a 3.2 mm HCN Cryo MAS probe. All experiments were conducted with 8 kHz MAS, and the microwave power at the probe was 10.5 W. During DNP experiments, the temperature was kept at around 105 K. Referencing for ^{13}C and ^{15}N was done indirectly to DSS using the low-field ^{13}C-signal of adamantane at 40.49 ppm. For all experiments, 100 kHz decoupling using SPINAL-64[64] was applied during acquisition. A recycle delay of 3 s was used.

2D ^{15}N–^{13}C correlation spectra were acquired using the z-filtered TEDOR sequence.[44] The length of the ^{1}H 90° pulse was 2.5 μs. ^{1}H–^{13}C-CP (cross-polarization) was applied with a contact time of 1000 μs. The pulse lengths of ^{13}C 90°, ^{13}C 180°, ^{15}N 90°, and ^{15}N 180° pulses were 4, 8, 7.5, and 15 μs, respectively. A total mixing time (τ_{mix}) of 6.25 ms (24 rotor cycles) was used for all experiments. The z-filter period was set to 250 μs. All 2D-spectra were acquired with 1024 scans in the direct dimension and 80 increments of 125 μs each in the indirect dimension. The FID acquisition time in the direct dimension was 10 ms. The ^{15}N pulse carrier was set to 111 ppm, close to the amide region, and the ^{13}C pulse offset was set to 68 ppm. During data processing, the direct ^{13}C

dimension was zero-filled to 8K complex data points followed by applying a Gaussian window function with 20 Hz line width. In the indirect ^{15}N dimension, 1K zero-filling followed by a squared-cosine window function is used prior to Fourier transformation.

1D ^{13}C–^{15}N TEDOR spectra were recorded with an initial ^{1}H–^{15}N-CP step using a 2.5 μs ^{1}H 90° pulse and a spin lock duration of 800 μs. The pulse lengths of ^{13}C 90°, ^{13}C 180°, ^{15}N 90°, and ^{15}N 180° pulses were 4, 8, 7.5, and 15 μs, respectively. The mixing time was varied between 0 and 80 rotor periods (0–20 ms). The ^{15}N FID was acquired for 10 ms. A total of 8192 scans were accumulated. The ^{15}N pulse carrier was set to the arginine resonance at 80 ppm and the ^{13}C pulse offset was set to 173 ppm. As reference, a ^{15}N-CP spectrum was recorded with the same settings and 128 scans. All spectra were processed with an exponential line broadening of 50 Hz.

For analyzing the buildup curve, the R51 signal was integrated from 60 to 90 ppm and plotted as a function of the mixing time. The integral intensity was normalized by the signal intensity observed under cross-polarization (Figure 6a). The ratio of the integral intensities of the backbone nitrogen resonance and the arginine peaks in the CP spectrum is 17.6:1. This corresponds well to the expected ratio of 18 obtained from the number of nitrogens contributing to both signals (275 × ^{15}N in the backbone vs 5 Arg with 3 × ^{15}N each). We can therefore assume that all five Arg contribute to the Arg resonance in the CP spectrum. The TEDOR signals were normalized by the integral Arg intensity observed in CP and corrected by the number of scans and by the total number of Arg per pentamer (25) and the number of TEDOR-active Arg per pentamer (1.25) according to $I_{CP}^{NORM} = (8192/128)(1.25/25)I_{CP}^{ARG}$. Jaroniec et al. have shown that multiple N–C distances can be extracted from TEDOR buildup curves obtained from ^{13}C coupled to multiple ^{15}N.[44] Here, all buildup curves overlap, as the ^{15}N resonances could not be deconvoluted. Therefore, fitting multiple distances to a single TEDOR buildup curve is not reliable. Instead, we have analyzed our data in terms of an effective dipole coupling, as explained above. The experimental buildup curve was fitted using the NonlinearModelFit routine within Mathematica (Wolfram Research) based on the analytical solutions for TEDOR signals provided by Müller.[65] Bessel functions were used up to an order of 5. Both D_{eff} and the single exponential relaxation damping parameter LB were freely varied until a global minimum was found. A RMSD contour plot is shown in Figure S5a (SI).

■ ASSOCIATED CONTENT

ⓢ Supporting Information

pH titration of λ_{max} of green PR in DDM, TX-100 and OG (Figure S1); statistical analysis of mixed labeled complexes (Table S1); supporting TEDOR spectra of green PR (Figure S2); supporting TEDOR spectra of GPR$_{R51A}$ and GPR$_{D52N}$ (Figure S3); statistical analysis of natural abundance spin pairs (Table S2); BN-PAGE, SEC, and pH titration of λ_{max} of GPR$_{R51A}$, GPR$_{D52N}$, GPR$_{E50Q}$ (Figure S4); RMSD contour plot for the analysis of TEDOR buildup data between R51 and D52′, geometry of both residues, and ^{15}N-T2′ data (Figure S5); analysis of cross-protomer salt bridges observed in blue PR X-ray structures (Table S3); BN-PAGE analysis of green PR reconstituted in DMPC and DOPC at two different LPRs using two different reconstitution methods (Figure S6). The Supporting Information is available free of charge on the ACS Publications website at DOI: 10.1021/jacs.5b03606.

■ AUTHOR INFORMATION

Corresponding Author

*glaubitz@em.uni-frankfurt.de

Notes

The authors declare no competing financial interest.

■ REFERENCES

(1) Ali, M. H.; Imperiali, B. *Biorg. Med. Chem.* **2005**, *13*, 5013.

(2) Doyle, D. A.; Morais Cabral, J.; Pfuetzner, R. A.; Kuo, A.; Gulbis, J. M.; Cohen, S. L.; Chait, B. T.; MacKinnon, R. *Science* **1998**, *280*, 69.

(3) Gurevich, V. V.; Gurevich, E. V. *Trends Neurosci.* **2008**, *31*, 74.

(4) Cymer, F.; Schneider, D. *Biol. Chem.* **2012**, *393*, 1215.

(5) Ernst, O. P.; Lodowski, D. T.; Elstner, M.; Hegemann, P.; Brown, L. S.; Kandori, H. *Chem. Rev.* **2014**, *114*, 126.

(6) Muller, D. J.; Sass, H. J.; Muller, S. A.; Buldt, G.; Engel, A. *J. Mol. Biol.* **1999**, *285*, 1903.

(7) Tsukamoto, T.; Kikukawa, T.; Kurata, T.; Jung, K. H.; Kamo, N.; Demura, M. *FEBS Lett.* **2013**, *587*, 322.

(8) Muller, M.; Bamann, C.; Bamberg, E.; Kuhlbrandt, W. *J. Mol. Biol.* **2015**, *427*, 341.

(9) Klyszejko, A. L.; Shastri, S.; Mari, S. A.; Grubmuller, H.; Muller, D. J.; Glaubitz, C. *J. Mol. Biol.* **2008**, *376*, 35.

(10) Ran, T.; Ozorowski, G.; Gao, Y.; Sineshchekov, O. A.; Wang, W.; Spudich, J. L.; Luecke, H. *Acta Crystallogr., Sect. D* **2013**, *69*, 1965.

(11) Gell, D. A.; Grant, R. P.; Mackay, J. P. *Adv. Exp. Med. Biol.* **2012**, *747*, 19.

(12) Morgner, N.; Kleinschroth, T.; Barth, H.-D.; Ludwig, B.; Brutschy, B. *J. Am. Soc. Mass Spectrom.* **2007**, *18*, 1429.

(13) Duarte, J. M.; Biyani, N.; Baskaran, K.; Capitani, G. *BMC Struct. Biol.* **2013**, *13*, 11.

(14) Tsuchiya, Y.; Nakamura, H.; Kinoshita, K. *Adv. Appl. Bioinform. Chem.* **2008**, *1*, 99.

(15) Carpenter, E. P.; Beis, K.; Cameron, A. D.; Iwata, S. *Curr. Opin. Struct. Biol.* **2008**, *18*, 581.

(16) Wang, S.; Ladizhansky, V. *Prog. Nucl. Magn. Reson. Spectrosc.* **2014**, *82*, 1.

(17) Hong, M. *Structure* **2006**, *14*, 1731.

(18) Carravetta, M.; Zhao, X.; Johannessen, O. G.; Lai, W. C.; Verhoeven, M. A.; Bovee-Geurts, P. H. M.; Verdegem, P. J. E.; Kiihne, S.; Luthman, H.; de Groot, H. J. M.; deGrip, W. J.; Lugtenburg, J.; Levitt, M. H. *J. Am. Chem. Soc.* **2004**, *126*, 3948.

(19) Jaroniec, C. P.; Lansing, J. C.; Tounge, B. A.; Belenky, M.; Herzfeld, J.; Griffin, R. G. *J. Am. Chem. Soc.* **2001**, *123*, 12929.

(20) Etzkorn, M.; Martell, S.; Andronesi, O. C.; Seidel, K.; Engelhard, M.; Baldus, M. *Angew. Chem., Int. Ed.* **2007**, *46*, 459.

(21) Shi, L.; Lake, E. M.; Ahmed, M. A.; Brown, L. S.; Ladizhansky, V. *Biochim. Biophys. Acta* **2009**, *1788*, 2563.

(22) Wang, S.; Munro, R. A.; Shi, L.; Kawamura, I.; Okitsu, T.; Wada, A.; Kim, S. Y.; Jung, K. H.; Brown, L. S.; Ladizhansky, V. *Nat. Methods* **2013**, *10*, 1007.

(23) Smith, S. O.; Song, D.; Shekar, S.; Groesbeek, M.; Ziliox, M.; Aimoto, S. *Biochemistry* **2001**, *40*, 6553.

(24) Wang, S.; Munro, R. A.; Kim, S. Y.; Jung, K.-H.; Brown, L. S.; Ladizhansky, V. *J. Am. Chem. Soc.* **2012**, *134*, 16995.

(25) Bayro, M. J.; Debelouchina, G. T.; Eddy, M. T.; Birkett, N. R.; MacPhee, C. E.; Rosay, M.; Maas, W. E.; Dobson, C. M.; Griffin, R. G. *J. Am. Chem. Soc.* **2011**, *133*, 13967.

(26) Van Melckebeke, H.; Wasmer, C.; Lange, A.; Eiso, A. B.; Loquet, A.; Bockmann, A.; Meier, B. H. *J. Am. Chem. Soc.* **2010**, *132*, 13765.

(27) Ni, Q. Z.; Daviso, E.; Can, T. V.; Markhasin, E.; Jawla, S. K.; Swager, T. M.; Temkin, R. J.; Herzfeld, J.; Griffin, R. G. *Acc. Chem. Res.* **2013**, *46*, 1933.

(28) Bajaj, V. S.; Mak-Jurkauskas, M. L.; Belenky, M.; Herzfeld, J.; Griffin, R. G. *Proc. Natl. Acad. Sci. U. S. A.* **2009**, *106*, 9244.

(29) Jacso, T.; Franks, W. T.; Rose, H.; Fink, U.; Broecker, J.; Keller, S.; Oschkinat, H.; Reif, B. *Angew. Chem., Int. Ed.* **2012**, *51*, 432.

(30) Ong, Y. S.; Lakatos, A.; Becker-Baldus, J.; Pos, K. M.; Glaubitz, C. *J. Am. Chem. Soc.* **2013**, *135*, 15754.

(31) Friedrich, T.; Geibel, S.; Kalmbach, R.; I, C.; Ataka, K.; Heberle, J.; Engelhard, M.; Bamberg, E. *J. Mol. Biol.* **2002**, *321*, 821.

(32) Beja, O.; Aravind, L.; Koonin, E. V.; Suzuki, M. T.; Hadd, A.; Nguyen, L. P.; Jovanovich, S. B.; Gates, C. M.; Feldman, R. A.; Spudich, J. L.; Spudich, E. N.; DeLong, E. F. *Science* **2000**, *289*, 1902.

(33) Gomez-Consarnau, L.; Akram, N.; Lindell, K.; Pedersen, A.; Neutze, R.; Milton, D. L.; Gonzalez, J. M.; Pinhassi, J. *PLoS Biol.* **2010**, *8*, e1000358.

(34) Bamann, C.; Bamberg, E.; Wachtveitl, J.; Glaubitz, C. *Biochim. Biophys. Acta* **2014**, *1837*, 614.

(35) Shi, L.; Ahmed, M. A.; Zhang, W.; Whited, G.; Brown, L. S.; Ladizhansky, V. *J. Mol. Biol.* **2009**, *386*, 1078.

(36) Hempelmann, F.; Holper, S.; Verhoefen, M. K.; Woerner, A. C.; Kohler, T.; Fiedler, S. A.; Pfleger, N.; Wachtveitl, J.; Glaubitz, C. *J. Am. Chem. Soc.* **2011**, *133*, 4645.

(37) Mao, J.; Do, N. N.; Scholz, F.; Reggie, L.; Mehler, M.; Lakatos, A.; Ong, Y. S.; Ullrich, S. J.; Brown, L. J.; Brown, R. C.; Becker-Baldus, J.; Wachtveitl, J.; Glaubitz, C. *J. Am. Chem. Soc.* **2014**, *136*, 17578.

(38) Mehler, M.; Scholz, F.; Ullrich, S. J.; Mao, J.; Braun, M.; Brown, L. J.; Brown, R. C.; Fiedler, S. A.; Becker-Baldus, J.; Wachtveitl, J.; Glaubitz, C. *Biophys. J.* **2013**, *105*, 385.

(39) Reckel, S.; Gottstein, D.; Stehle, J.; Lohr, F.; Verhoefen, M. K.; Takeda, M.; Silvers, R.; Kainosho, M.; Glaubitz, C.; Wachtveitl, J.; Bernhard, F.; Schwalbe, H.; Guntert, P.; Dotsch, V. *Angew. Chem., Int. Ed.* **2011**, *50*, 11942.

(40) Hoffmann, J.; Aslimovska, L.; Bamann, C.; Glaubitz, C.; Bamberg, E.; Brutschy, B. *Phys. Chem. Chem. Phys.* **2010**, *12*, 3480.

(41) Edwards, D. T.; Huber, T.; Hussain, S.; Stone, K. M.; Kinnebrew, M.; Kaminker, I.; Matalon, E.; Sherwin, M. S.; Goldfarb, D.; Han, S. *Structure* **2014**, *22*, 1677.

(42) Stone, K. M.; Voska, J.; Kinnebrew, M.; Pavlova, A.; Junk, M. J. N.; Han, S. G. *Biophys. J.* **2013**, *104*, 472.

(43) Hing, A. W.; Vega, S.; Schaefer, J. *J. Magn. Reson.* **1992**, *96*, 205.

(44) Jaroniec, C. P.; Filip, C.; Griffin, R. G. *J. Am. Chem. Soc.* **2002**, *124*, 10728.

(45) Sauvee, C.; Rosay, M.; Casano, G.; Aussenac, F.; Weber, R. T.; Ouari, O.; Tordo, P. *Angew. Chem., Int. Ed.* **2013**, *52*, 10858.

(46) Wittig, I.; Braun, H.-P.; Schaegger, H. *Nat. Protoc.* **2006**, *1*, 418.

(47) Kunji, E. R. S.; Harding, M.; Butler, P. J. G.; Akamine, P. *Methods* **2008**, *46*, 62.

(48) Hussain, S.; Kinnebrew, M.; Schonenbach, N. S.; Aye, E.; Han, S. *J. Mol. Biol.* **2015**, *427*, 1278.

(49) Lipfert, J.; Columbus, L.; Chu, V. B.; Lesley, S. A.; Doniach, S. *J. Phys. Chem. B* **2007**, *111*, 12427.

(50) Paradies, H. H. *J. Phys. Chem.* **1980**, *84*, 599.

(51) Dioumaev, A. K.; Brown, L. S.; Shih, J.; Spudich, E. N.; Spudich, J. L.; Lanyi, J. K. *Biochemistry* **2002**, *41*, 5348.

(52) Zorin, V. E.; Brown, S. P.; Hodgkinson, P. *Mol. Phys.* **2006**, *104*, 293.

(53) Zorin, V. E.; Brown, S. P.; Hodgkinson, P. *J. Chem. Phys.* **2006**, *125*, 144508.

(54) Fotiadis, D.; Liang, Y.; Filipek, S.; Saperstein, D. A.; Engel, A.; Palczewski, K. *Nature* **2003**, *421*, 127.

(55) Fung, J. J.; Deupi, X.; Pardo, L.; Yao, X. J.; Velez-Ruiz, G. A.; DeVree, B. T.; Sunahara, R. K.; Kobilka, B. K. *EMBO J.* **2009**, *28*, 3315.

(56) Ernst, O. P.; Gramse, V.; Kolbe, M.; Hofmann, K. P.; Heck, M. *Proc. Natl. Acad. Sci. U. S. A.* **2007**, *104*, 10859.

(57) Lorch, M.; Booth, P. J. *J. Mol. Biol.* **2004**, *344*, 1109.

(58) Schafer, G.; Shastri, S.; Verhoefen, M. K.; Vogel, V.; Glaubitz, C.; Wachtveitl, J.; Mantele, W. *Photochem. Photobiol.* **2009**, *85*, 529.

(59) Wang, N.; Wang, M.; Gao, Y.; Ran, T.; Lan, Y.; Wang, J.; Xu, L.; Wang, W. *Acta Crystallogr., Sect. F* **2012**, *68*, 281.

(60) Mors, K.; Roos, C.; Scholz, F.; Wachtveitl, J.; Dotsch, V.; Bernhard, F.; Glaubitz, C. *Biochim. Biophys. Acta* **2013**, *1828*, 1222.

(61) Ranaghan, M. J.; Schwall, C. T.; Alder, N. N.; Birge, R. R. *J. Am. Chem. Soc.* **2011**, *133*, 18318.

(62) Morgner, N.; Barth, H. D.; Brutschy, B. *Aust. J. Chem.* **2006**, *59*, 109.

(63) Morgner, N.; Hoffmann, J.; Barth, H. D.; Meier, T.; Brutschy, B. *Int. J. Mass Spectrom.* **2008**, *277*, 309.

(64) Fung, B.; Khitrin, A.; Ermolaev, K. *J. Magn. Reson.* **2000**, *142*, 97.

(65) Mueller, K. T. *J. Magn. Reson., Ser. A* **1995**, *113*, 81.